ISSN: 0067-2904

Removing of Copper ions from Industrial Wastewater Using Graphene oxide/Chitosan Nanocomposite

Hakim H. Kadhim*, Khulood A. Saleh
Department of Chemistry, College of Science, University of Baghdad, Baghdad, Iraq

Received: 8/5/2021 Accepted: 1/9/2021 Published: 30/5/2022

Abstract

A simple method was used to create a graphene oxide/chitosan (GO/CS) nanocomposite, which was then used in batch experiments to remove copper ions from industrial wastewater under various conditions of initial concentration, adsorbent weight, pH, and contact time. Maximum removal percentage equal to 99.4 % for initial copper ion concentration of $5x10^{-2}$ mol/L at pH 6, time 75 min, temperature 25 °C, and adsorbing dose 0.1 g. The pseudo-second order kinetic model and the Freundlich isotherm adequately fit the experimental results. The process was spontaneous and endothermic, according to thermodynamic studies.

Keywords: Graphene oxide/chitosan nanocomposite, Adsorption, Copper, kinetic, Thermodynamic.

إزالة أيونات النحاس من مياه الصرف الصناعي باستخدام المركب اوكسيد الكرافين/الشيتوزان النانوي

حكيم حيال كاظم*, خلود عبد صالح

قسم الكيمياء, كلية العلوم, جامعة بغداد, بغداد, العراق

الخلاصة

تم استخدام طريقة بسيطة لإنشاء متراكب نانوي من أكسيد الجرافين / الشيتوزان (GO / CS) ، والذي تم استخدامه بعد ذلك في تجارب دفعية لإزالة ايونات النحاس من مياه الصرف الصناعي في ظل ظروف مختلفة من التركيز الأولي ، وزن المادة المازة ، الدالة الحامضية ووقت التلامس. نسبة الازالة القصوى تساوي 99.4% لتركيز أيونات النحاس الأولي $5x10^{-2}$ مول / لتر عند الأس الهيدروجيني 6 ، الوقت 75 دقيقة ، درجة الحرارة 25 درجة مئوية وجرعة الامتزاز 0.1 غرام . تتناسب النتائج التجريبية مع النموذج الحركي من المرتبة الثانية الكاذبة ومع نموذج متساوي درجة الحرارة فريندلش . كانت العملية تلقائية وماصة للحرارة ، وفقًا لدراسات الثرموديناميك.

1. Introduction

Wastewater is a huge environmental pollution, as it is considered a mixture of liquid and solid materials that comes after the use of water in homes, industries and commercial establishments [1]. The wastewater from electroplating, electrolysis, coatings, textiles, pesticides, pharmaceuticals, paper-making, printing, dyeing, and other chemical industries have caused great damage to the natural environment [2]. Copper is a common component of wastewater in manufacturing industries, such as mining mineral processing, and other processing industries [3]. Because of its high concentrations, copper content is easily detectable in wastewater produced in industrial applications, and it is one of the most

*Email: hhk92.hh@gmail.com

commonly used heavy metals in most industry sectors. Copper, for example, can be used in electroplating, plastics, etching, and, finally, metal finishing and processing [4]. Copper concentrations in the effluent stream
are high enough to damage the brain, kidneys, and cause anemia. At large doses, copper may be stored in the brain, kidneys, skin, and liver, raising serious toxicological problems [5]. According to World Health Organization (WHO) and Environmental Protection Agency (EPA), the permissible limit of copper ions in consumable water is 1.5 mg/L and 1.3 mg/L, respectively [6]. Several methods for removing heavy metals from wastewater have been investigated over the last decade, including adsorption, precipitation, ion exchange, membrane process, electrocoagulation, and electrodeposition [7-9]. Among the above-mentioned methods, adsorption has inherent benefits such as low cost, high removal rate, ease of access, and less secondary pollution [10]. Different types of natural adsorbents are used for the removal of metal ions from wastewater. Chitosan (CS) is a substance derived primarily from chitin, a carbohydrate found in the outer shells of seafood such as shrimp and crustaceans [11,12]. CS is a bio-adsorbent and disinfectant material that is inexpensive and has numerous advantages such as the amine functional group, which is completely reactive among metal ions, biocompatibility, biodegradability, and their safe use due to their non-toxic behavior [13].

Graphene oxide (GO) has demonstrated a high efficiency in the removal of pollutant metal ions and toxic contaminants from water as a two-dimensional carbon material with numerous functional groups on its basal plans and corners [14,15]. Heavy metal complexes may be able to bind to functional groups containing oxygen. Furthermore, because of the large total area available, GO is an excellent candidate for water purification [16]. It has been proposed that GO could be a good adsorbent for removing dyes, heavy metals, and organic pollutants with high speed and efficiency [17]. The graphene oxide/chitosan mixture improves its adsorbent properties as binding power, selectivities and mechanical properties, which are important for improving the performance of heavy metal adsorption [18].

In this work, we study the efficiency of GO/CS nanocomposite for copper removal from industrial wastewater under different conditions such as pH, initial concentration, adsorbent dose and contact time. The adsorption data have been tested using Langmuir and Freundlich isothermal adsorption, and thermodynamic parameters were also calculated. The kinetic data is analyzed using a pseudo-first order and pseudo-second order equations.

2. Materials and methods

2.1. Materials

Chitosan (≥ 90% deacetylation) were supplied by Cheng Du Micxy Chemical Co.,Ltd (Cheng Du, China). Copper sulphate, Hydrochloric acid, Sodium hydroxide, Sulphuric acid were supplied by BDH. All of the reagents have been analytical grade and were used exactly as they were received, with no purification.

2.2. Graphene oxide (GO) preparation

Hummers and Offema method are used to create GO from graphite [19]. Briefly, 1.0 g of graphite was added to a 250 mL beaker, followed by 0.5 g of $NaNO_3$ and 23 mL of concentrated H_2SO_4 while stirring in an ice bath. Then, 3.0 g of $KMnO_4$ was slowly added with stirring and cooling to keep the reaction mixture temperature below 20 °C. The ice bath was removed after 5 min, and the system has been heated to 35°C for 30 min. After that, 50 mL of water was slowly added to the system, and the mixture was stirred for 15 min at 90°C. 166 mL of water was added and followed by a slow addition of 5 mL of 30% H_2O_2, turning the color of the solution to dark brown. The solid product was separated, and washed with 85 mL of 4% HCl aqueous solution followed by washing with 65 mL of water to remove the acid. Then, the solution was separated, and the residue was washed with water until the pH of the suspension's upper layer was near to 7 and dried overnight at room temperature.

2.3. Preparation of graphene oxide/chitosan (GO/CS) nanocomposite

GO/CS nanocomposite was prepared as followed [20]. 0.1 g GO was dispersed in 20 mL water and treated with ultrasound for 1 h to obtain the GO suspension. The CS solution was prepared by dissolving 0.5 g CS powder into 100 mL of 2% acetic acid aqueous. The CS solution and the GO suspension were vigorously mixed together. To make the homogeneous GO/CS solution, the obtained solution was treated with ultrasound for an additional 1 h and stirred for 12 h. Then, dried overnight at room temperature.

2.4. Characterization

FTIR spectra of GO, CS, and GO/CS nanocomposite were measured by using a Shimadzu IRAffinity-1 FTIR Spectrophotometer (Shimadzu Corp., Japan). The spectral scan ranged between 400 and 4000 cm^{-1}. The X-ray diffraction (XRD) pattern of GO, CS, and GO/CS nanocomposite were studied using a Shimadzu XRD-6000 X-ray diffractometer (Shimadzu, Japan) in the 5–80° (2θ) range with Cu Kα (λ=1.5406 A^o), worked at 100 mA and 40KV.

2.5. Adsorption experiments

The stock solution of copper sulfate $CuSO_4.5H_2O$ 0.1 mol/L was prepared by dissolving 12.48 g of copper sulfate in 500 mL of distilled water and then dilution to required concentration. Adsorption experiments were done using a batch model, containing a copper sulfate (50 mL) solution at an initial concentration from $5x10^{-2}$ to $1x10^{-4}$ mol/L in series of conical flasks (250 mL). For pH adjustment, HCl (0.1M) and NaOH (0.1M) solutions were used. To achieve equilibrium, 0.1 g of GO/CS powder was added to copper solution and stirred constantly for 75 min. After centrifuging the mixture for 5 min, the amount of copper adsorbed was determined using an atomic absorption spectrophotometer (AAS) (Model: AA-7000, Shimadzu). Equations were used to measure the copper removal percentage and equilibrium uptake [21]:

$$\%Removal = \frac{C_o - C_e}{C_o}\ 100 \quad (1)$$

$$q_e = \frac{C_o - C_e}{M}\ V \quad (2)$$

Where, C_o is the initial concentration (mol/L), M (g) adsorbent weight, C_e is equilibrium concentration (mol/L), and V the volume of the solution in liters.

3. Results and Discussion

3.1. Characterization study

Figure 1 depicts the major GO absorption bands in the FTIR spectrum, which appear at 3414.0, 3022.45, 1716.65, 1627.92, 1290.38, 1155.36, and 1087.85 cm^{-1}. The OH groups are represented by the absorption band at 3414.0 cm^{-1}, whereas the C-H stretch of GO is represented by the band at 3022.45 cm^{-1}. The FTIR spectrum of GO shows a peak at 1716.65 cm^{-1} due to the C=O stretching vibration of the COOH groups and a peak at 1627.92 cm^{-1} due to the C=C expansion mode of the sp^2 carbon skeleton network or epoxy groups. Furthermore, peaks of absorption observed at 1290.38, 1155.36, and 1087.85 cm^{-1} can be attributed to the C-O vibration of various oxygen-containing groups such as carboxyl and epoxy groups [22]. Figure 2 depicts the FTIR spectra of CS. A broad band appears in the CS spectrum at 3441.01 cm^{-1}, which corresponds to the stretching vibrations of the O-H and N-H groups. A peak at 2889.37 cm^{-1} can be characterized for C-H extending the aliphatic group's vibration. The C=O stretching vibration (amide I band) and C-N stretching vibration (amide III band) in amide groups are represented by the absorption bands at 1654.92 cm^{-1} and 1379.1 cm^{-1}, respectively. The N-H bending vibration and N-H deformation vibration occurs at 1597.06 cm^{-1} and 1421.54 cm^{-1} in the primary amine groups (-NH_2). Other significant absorption bands in CS can be found at 1323.17 cm^{-1} (C-N stretching vibration), 1153.43 cm^{-1} (anti-symmetrical stretching vibration of the C-O-C bridge), 1072.42 cm^{-1} (C-O stretching vibration of a saccharide structure), and 1031.92 cm^{-1} (O-H bending vibration) [20] . As shown in Figure 3, the combination of GO and CS has resulted in many changes to the FTIR spectrum of the

GO/CS nanocomposite. The peak of COOH at 1716.65 cm^{-1} (from GO spectrum) and the peak of NH_2 at 1597.06 cm^{-1} (from CS spectrum) have both vanished. Meanwhile, amides (C=O stretching vibrations of –NHCO) were discovered in a new absorption band at 1635.64 cm^{-1}. This finding is linked to the reaction of GO carboxyl groups with CS amino groups. A new band at 1556.55 cm^{-1} could be attributed to the reaction of CS amino groups and GO epoxy groups to form amide II groups [22].

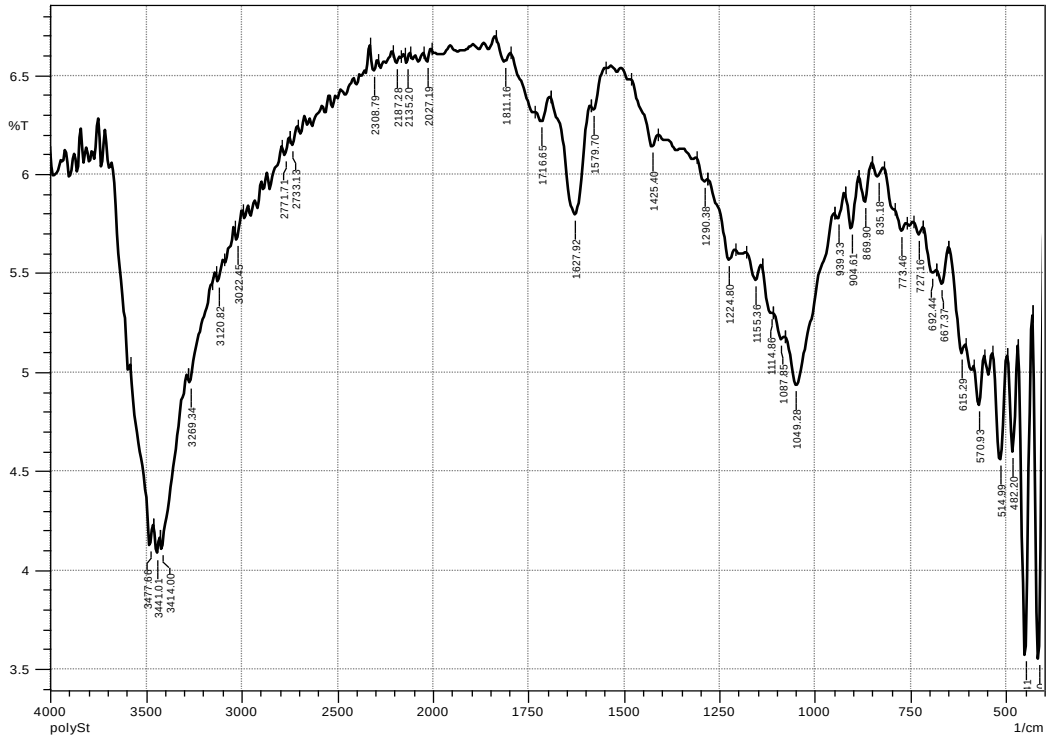

Figure 1- FTIR spectrum of GO.

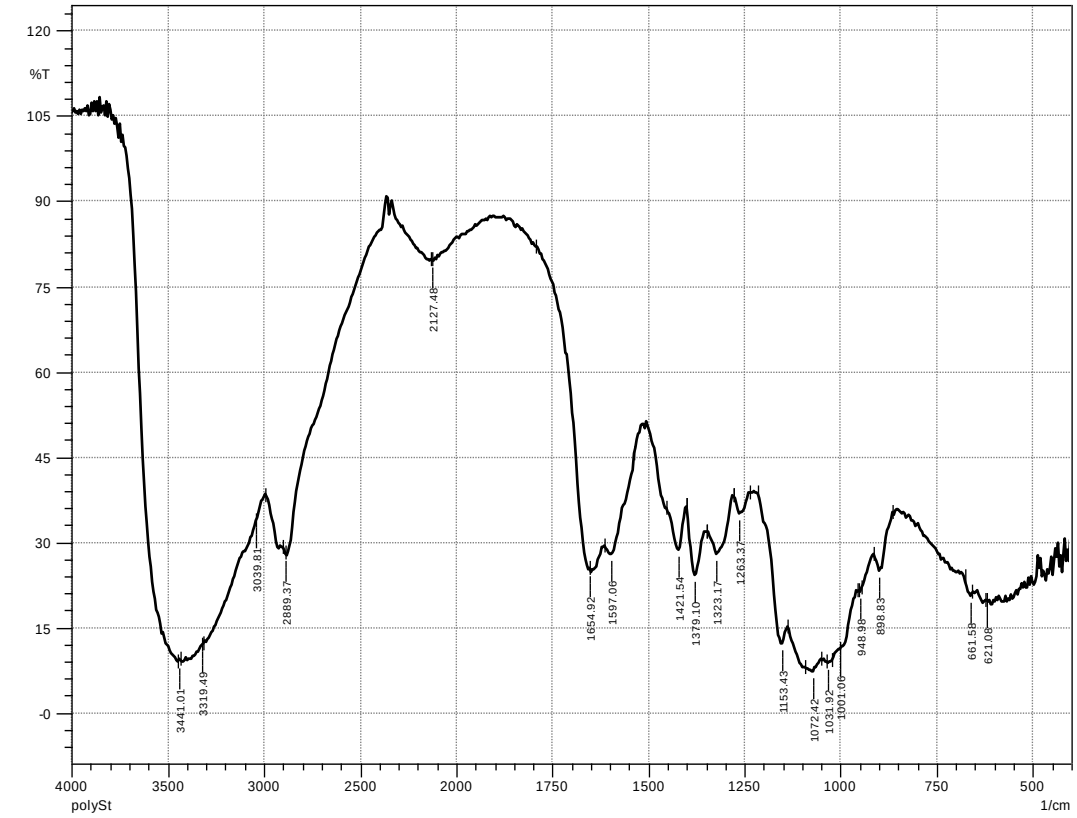

Figure 2- FTIR spectrum of CS.

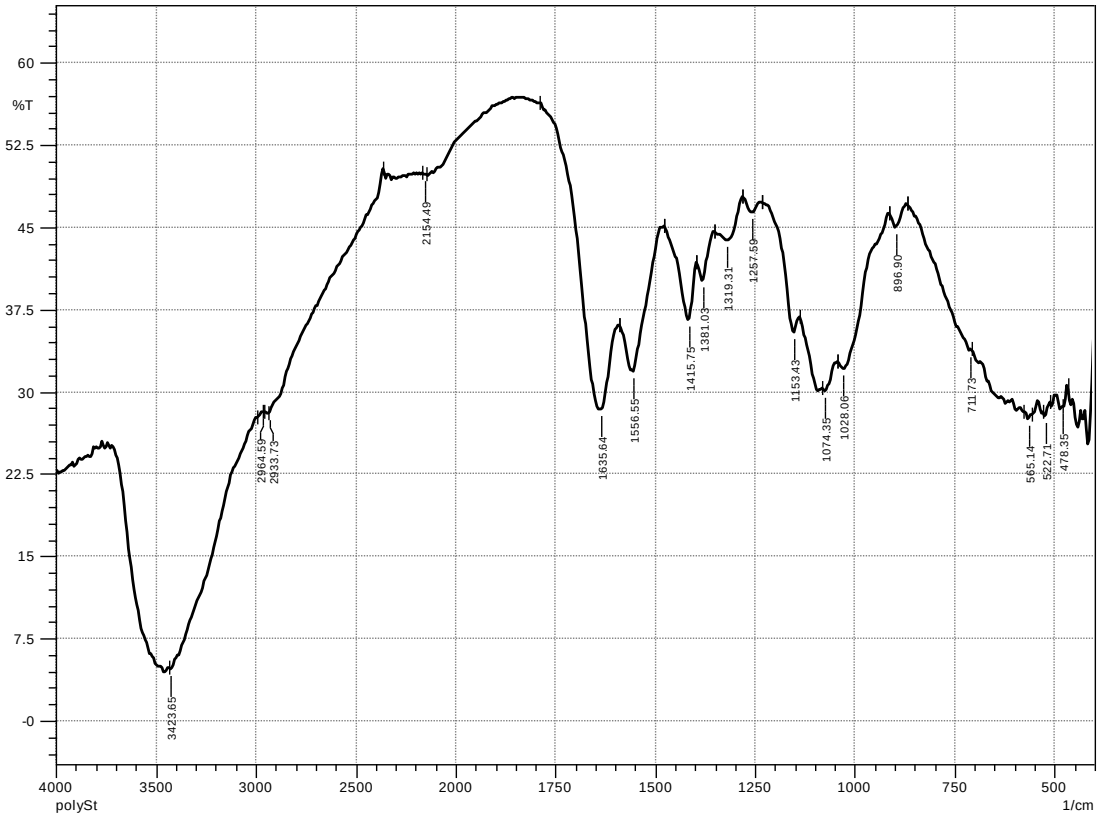

Figure 3- FTIR spectrum of GO/CS nanocomposite.

XRD patterns of GO, CS, and GO/CS nanocomposites are shown in Figure 4. XRD of GO (Figure 4A) shows a strong peak at $2\theta=10.49^{o}$, which corresponds to (001) plane diffraction of GO, which has a d-spacing of 8.42 A^{o}, as estimated by Braggs equation [23]:

$$n\lambda = 2d\sin\theta \quad (3)$$

Where, θ is the beam diffraction angel with respect to the crystalline plane, n is integer number, λ is the wave length of X-Ray incident beam and d is distance between the entire structural planes. The average particle sizes were estimated using Scherrer equation [24]:

$$\beta = K\lambda / D\cos\theta \quad (4)$$

Where, K is the Scherrer constant which depends on the shape of the peak, λ represents the wavelength of X-ray incident beam, D is the size of the crystal structure, and θ represents the Bragg's angle.

Figure 4B shows XRD pattern of CS sample, the characteristic peaks of CS are located at $2\theta =12.3^{o}$ and 20.2^{o}, which are assigned to JCPDS card No. 039–1894 [25]. Furthermore, two peaks were produced at 2θ=12.17° and 22.05° after synthesizing GO with CS. XRD patterns of GO/CS (Figure 4C) are slightly different from those of CS, which indicates that GO nanosheets were distributed uniformly within CS polymer. The absence of the typical GO peak ($2\theta=10.49^{o}$), indicates that the majority of GO reacted with CS. The amine groups of CS reacted with the carbonyl and epoxyl groups of GO, and thus may have influenced on the layered structure and crystallization property [26].

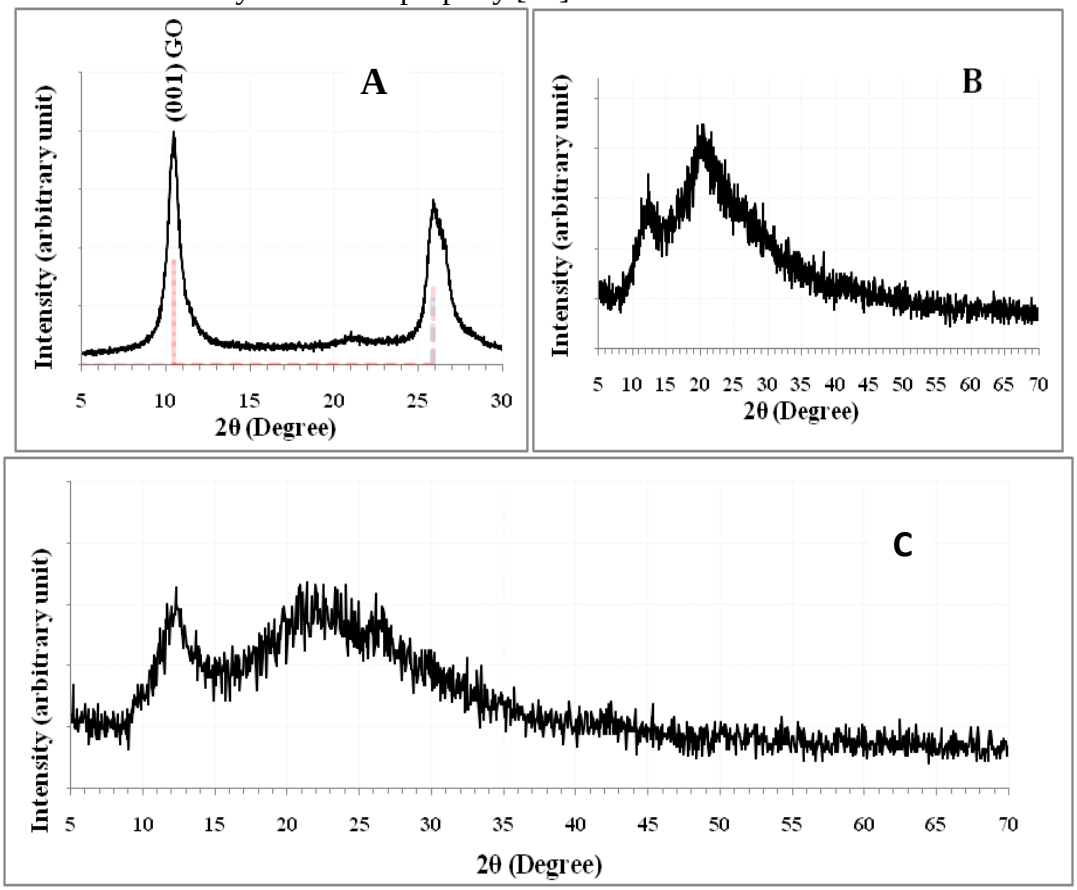

Figure 4- XRD patterns of A) GO, B) CS, C) GO/CS.

Table 1 shows the XRD parameters for GO, CS, and GO/CS which were obtained using Braggs and Scherrer equations (3) and (4).

Table 1- XRD parameters for GO, CS, and GO/CS.

Samples	2θ (Deg.)	FWHM (Deg.)	d_{hkl} Exp.(A°)	C.S (nm)	hkl	No of layers
GO	10.490	0.742	8.4264	10.752	(001)	13
CS	12.376	2.561	7.1462	3.120	(111)	4
	20.264	6.454	4.3788	1.250	(200)	3
GO/CS	12.171	1.9464	7.2661	4.105	(002)	6
	22.057	6.966	4.0267	1.162	(101)	3

3.2. Effect of pH

The pH of the solution had an effect on the electrical charge of the adsorbent surface as well as the ionic forms of the adsorbate molecule. As a result, as the acidity decreases, the adsorption of Cu (II) increases, since the hydrogen ion competes with the Cu (II) molecule in acid medium, and as the number of hydrogen ions decreases, more adsorption sites become available to adsorb Cu (II) [27]. The optimal pH, as shown in Figure 5, is 6. Adsorption studies could not be performed at pH values greater than 6 due to $Cu(OH)_2$ precipitation.

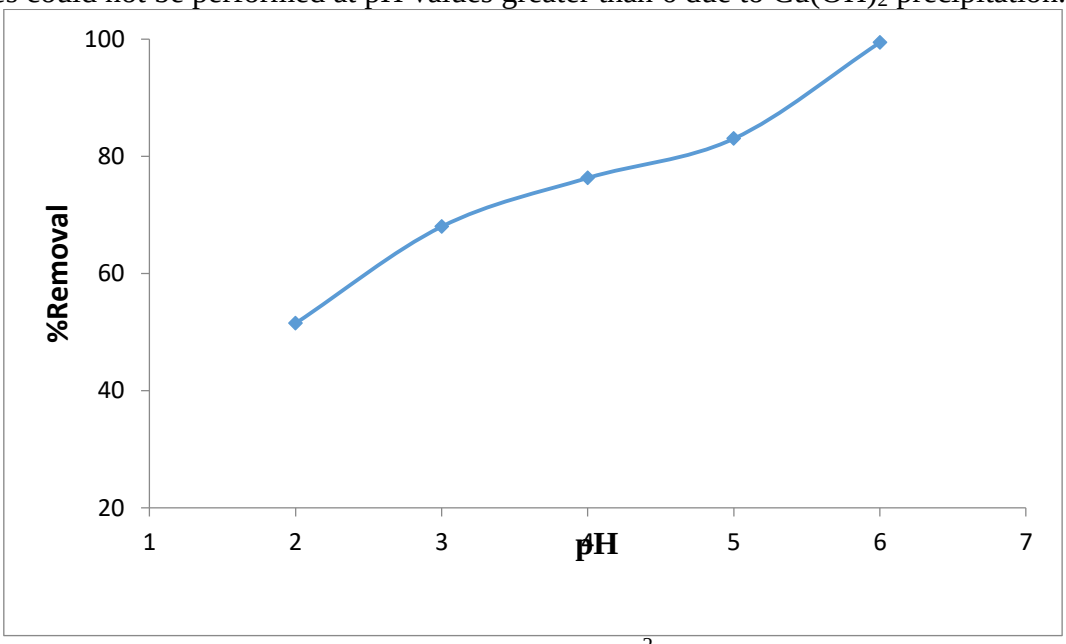

Figure 5- Effect of pH on percentage removal of $5x10^{-2}$ mol/L initial concentration of Cu (II) at 298K.

3.3. Effect of adsorbent weight

The effect of different GO/CS weights on Cu (II) percentage removal at a contact time of 75 min was investigated by varying the GO/CS weight in 50 ml of $1x10^{-3}$ mol/L copper solution from 0.05g to 0.25g. Figure 6 shows increased percentage removal as GO/CS weight increases, Since increasing the GO/CS weight results in a greater number of adsorbent sites, more surface area means a greater number of adsorbent sites [28].

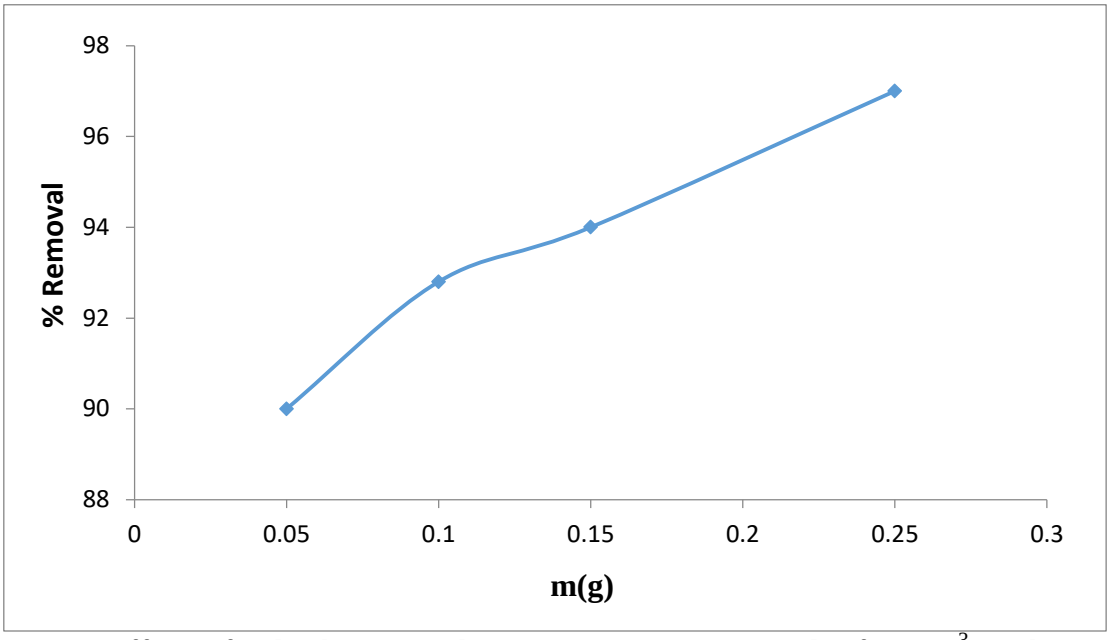

Figure 6- Effect of adsorbent weight on percentage removal of $1x10^{-3}$ mol/L initial concentration of Cu (II) at 298 K.

3.4. Effect of initial concentration

To demonstrate the effect of the initial copper concentration, different concentrations ($5x10^{-2}$, $1x10^{-2}$, $5x10^{-3}$, $1x10^{-3}$, $5x10^{-4}$ and $1x10^{-4}$) mol/L were used at 298K, adsorbent weight (0.1 g), and shaking period 75 min. Figure 7 shows that when the initial copper concentration increased, the removal efficiency is also increased. At a low concentration, the ratio of number of active sites that available per unit copper concentration was a small may be due to increased competition for active sites [29]. Thus, the adsorption became independent of initial concentration. As the initial copper concentration rises, so do the interaction forces, which are critical for overcoming the resistance to mass transfer between copper and the GO/CS [30]. After that, as the initial copper concentration increased, most of the active sites became occupied, resulting in a slight increase in removal efficiency.

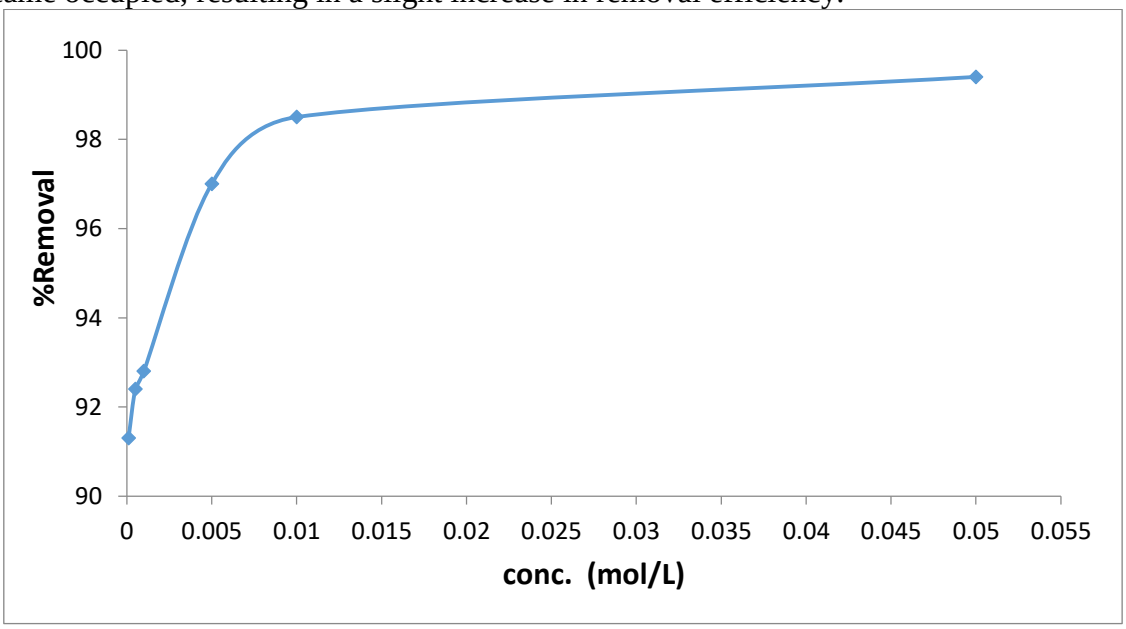

Figure 7- Effect of initial concentration on percentage removal of Cu (II) at 298K.

3.5. Effect of contact time

The effect of contact time between the GO/CS and copper on the removal percentage was determined at $5x10^{-4}$ mol/L initial copper concentration, 0.1g adsorbent weight, and 298K. Figure 8 shows the removal percentage increasing with time, and after 75 minutes, the amount of copper adsorbed on the adsorbent is equal to the amount of copper desorbed from the adsorbent.

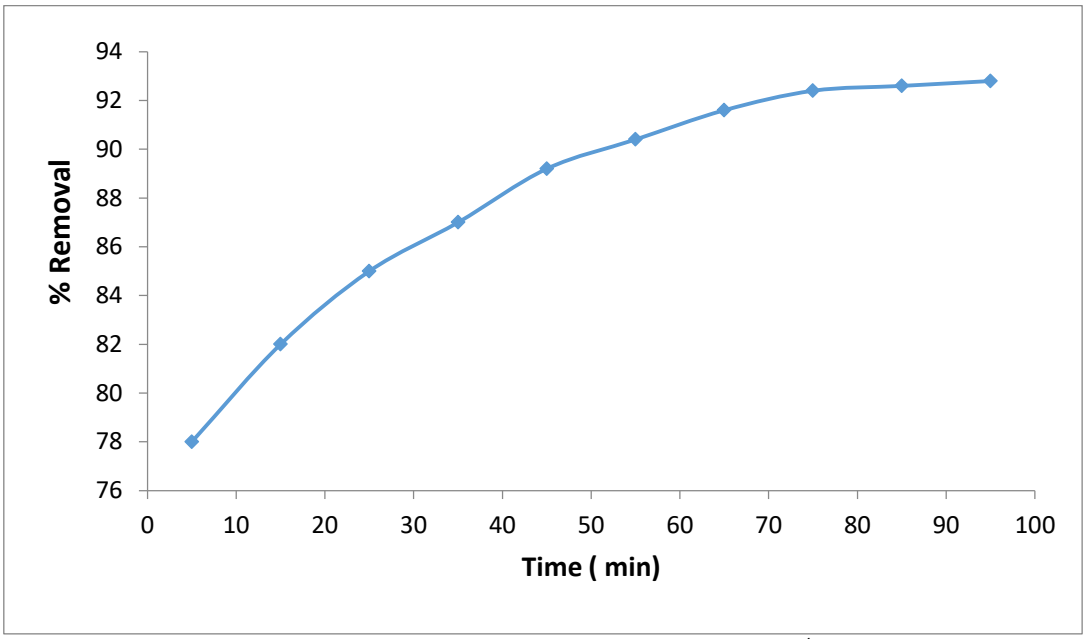

Figure 8- Effect of contact time on percentage removal of $5x10^{-4}$ mol/L Cu (II) at 298K.

3.6. Equilibrium isotherm

The isotherm of adsorption describes the relation between the number of copper molecules adsorbed by adsorbent mass and their balance at a constant temperature. Adsorption isotherms are a must-have for any adsorption system's design**.** The isotherms were studied using 50 ml of copper solution with different concentrations ($5x10^{-2}$, $1x10^{-2}$, $5x10^{-3}$, $1x10^{-3}$, $5x10^{-4}$ and $1x10^{-4}$) mol/L at different temperatures (298, 308, 318 and 328) K. In this study, the well-known equilibrium model by Langmuir and Freundlich is used. The Langmuir model predicts a homogeneous distribution of adsorbate on the adsorbent's surface, as well as an energetically similar monolayer or single layer of adsorption sites, with no interaction between adsorbed ions even at adjacent sites [31]. Freundlich isotherm model expression defines surface heterogeneity as well as the exponential distribution of active sites and active site energies [32]. The linear form of Langmuir equation and separation factor are given by following equations [31]:

$$\frac{C_e}{q_e} = \frac{C_e}{q_m} + \frac{1}{K_L q_m} \quad (5)$$

$$R_L = \frac{1}{1+K_L C_o} \quad (6)$$

Where, C_e is equilibrium concentration of adsorbate (mol/L), q_e is the amount of adsorbed at equilibrium time (mol/g), K_L is Langmuir isotherm constant (L/mol), and q_m is the maximum adsorption capacity (mol/g). The slope and intercept of the plot between C_e/q_e versus C_e will give q_m and K_L respectively as shown in Figure 9. These results were similar to those obtained by Belbachir and Makhoukhi [33]. And the value of Langmuir constants K_L and C_o initial copper concentration are submitted in Equation (4) to calculate the separation constant R_L the value was found in favorable range ($0<R_L<1$) this indicate favorable adsorption of copper onto GO/CS.

The Freundlich adsorption isotherm model is represented as follows [34]:

$$logq_e = logK_F + \frac{1}{n} logC_e \quad (7)$$

Where, q_e is the amount of adsorbed at equilibrium time (mol/g), C_e is equilibrium concentration of adsorbate (mol/L), K_F the adsorption capacity constant (mol/g),1/n the adsorption intensity of the adsorbate towards the adsorbent or heterogeneity. The slope and intercept of the plot between log q_e versus log C_e will give 1/n and K_F respectively as shown in Fiqure 10. When 1/n = 1, the partition between the two phases is concentration independent. When the value of 1/n is less than one, this indicates (a normal adsorption). When 1/n values are greater than one, this indicates (a cooperative adsorption) [35,36]. The data in Table 2 show the adsorption of copper on GO/CS follows the Freundlich model (R^2 =0.930).

Table 2- Isotherms constants and correlation coefficient

Temp. (K)	Lanqmuir isotherm			Freundlich isotherm		
	K_L (L/mol)	q_m (mol/g)	R^2	K_F (mol/g)	1/n	R^2
298	3903.2	$148x10^{-5}$	0.833	16557.6	1.740	0.929
308	6060.6	$103x10^{-5}$	0.913	61235.0	1.827	0.889
318	6756.7	$106x10^{-5}$	0.908	58076.4	1.820	0.889
328	9881.4	$112x10^{-5}$	0.707	346736.8	1.898	0.930

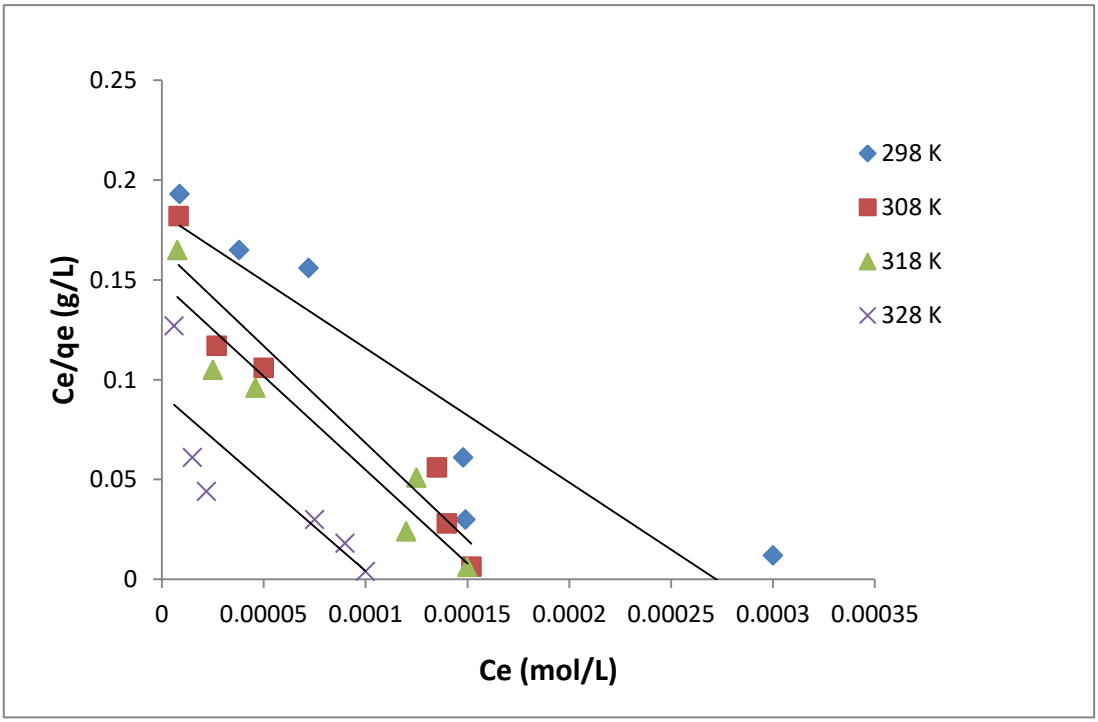

Figure 9- Langmuir adsorption isotherm of Cu (II) onto GO/CS.

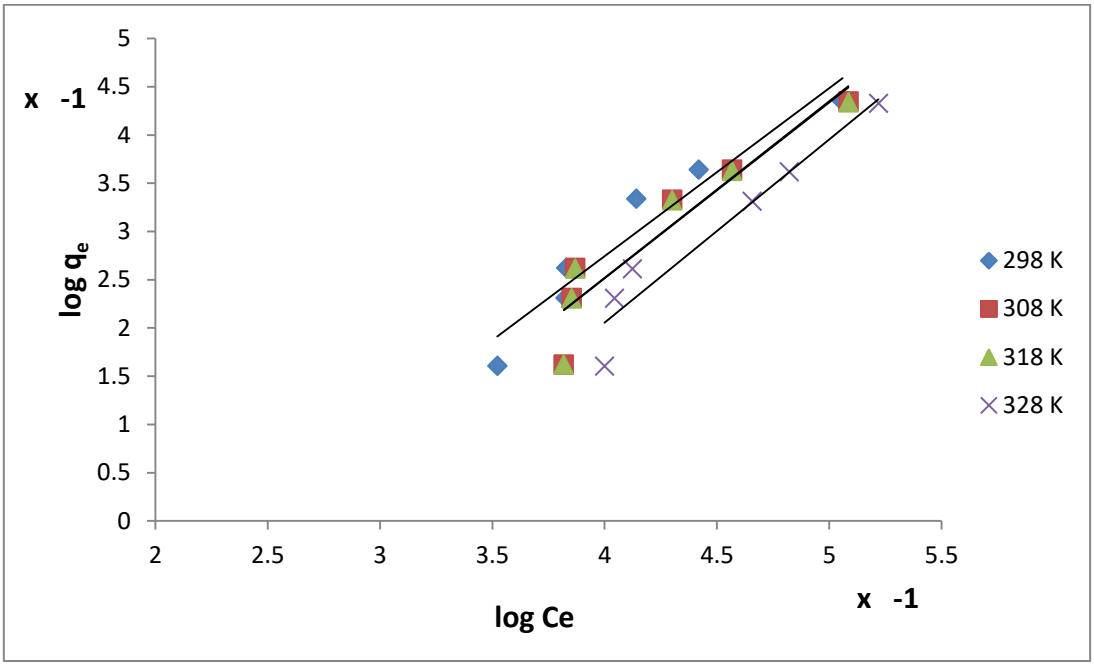

Figure 10- Freundlich adsorption isotherm of Cu (II) onto GO/CS.

3.7. Adsorption Kinetics

Kinetics of Adsorption and Adsorption process control mechanisms are noted and essential to designating the time and rate of adsorption in order to enhance the understanding of the adsorption process [31,37]. There are few adsorption kinetic models such as pseudo-first order and pseudo-second order. The linear form of pseudo-first order is expressed as follows [38]:

$$\log(q_e - q_t) = log\, q_e - \frac{k_1}{2.303} t \quad (8)$$

Where, k_1 is the rate constant of the pseudo-first-order adsorption model (min^{-1}) q_e and q_t is the amount of adsorbed (mol/g) at equilibrium and at the time t (min). The slope and intercept of the plot between log (q_e-q_t) versus t will give k_1 and q_e respectively as shown in Fiqure 11. A pseudo-second order equation can be presented in a linear form as follows [39]:

$$\frac{t}{q_t} = \frac{1}{k_2 q_e^2} + \frac{t}{q_e} \quad (9)$$

Where, k_2 is the equilibrium rate constant of pseudo-second order (g/mol min). The slope and intercept of the plot between t/q_t versus t will give q_e and k_2 respectively. The following equation relates the initial adsorption rate h_o at different initial concentrations [40]:

$$h_o = k_2 q_e^2 \quad (10)$$

The comparison of kinetic constants and correlation coefficients of kinetic models shows that the pseudo-second order model fits better, as shown in Table 3.

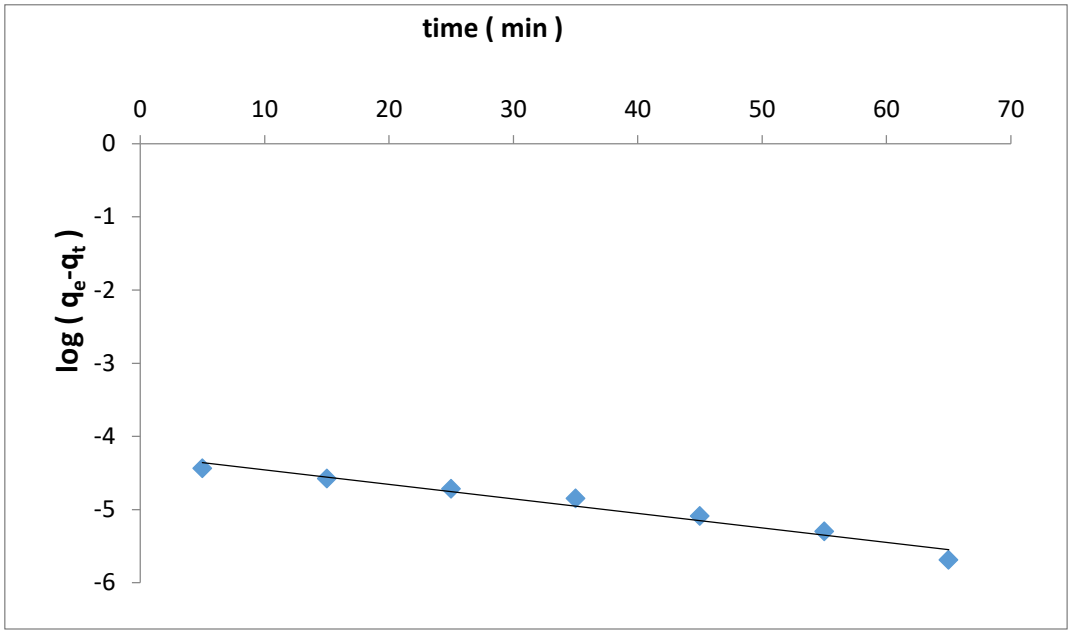

Figure 11- Pseudo-first order of Cu(II) onto GO/CS at 298K.

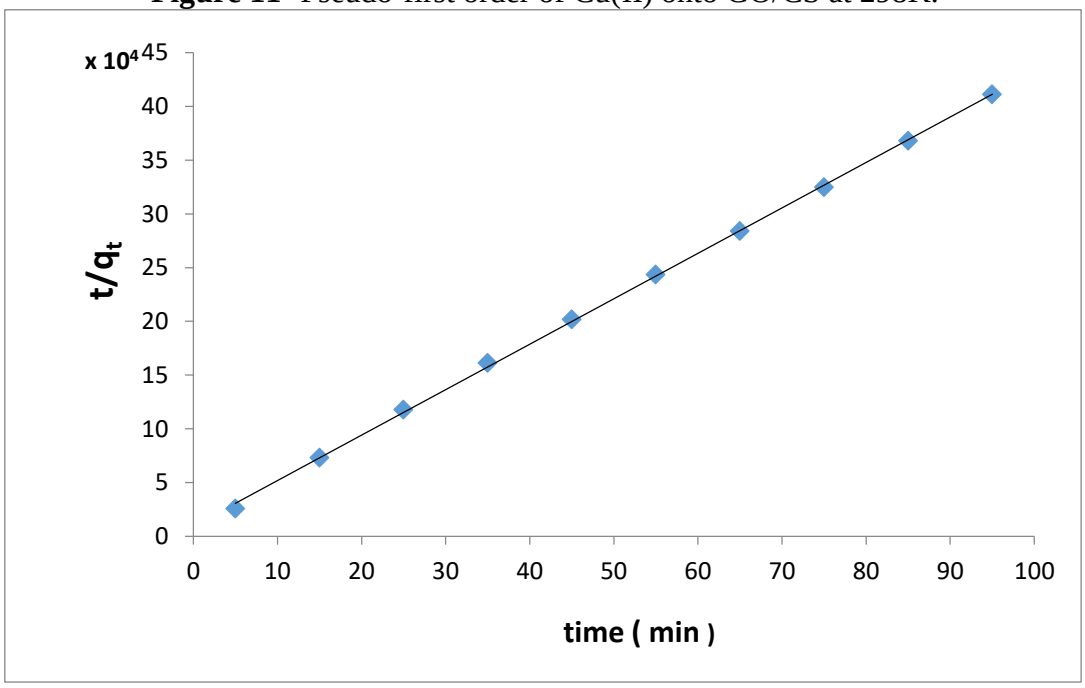

Figure 12- Pseudo-second order of Cu(II) onto GO/CS at 298K.

Table 3- Kinetic results of 5x10^{-4} Cu(II) on GO/CS at 298K.

$q_{e,exp.}$ (mol/g)	Pseudo-first order			Pseudo-second order		
	k_1 (min^{-1})	$q_{e,cal}$ (mol/g)	R^2	k_2 (g/mol.min)	$q_{e,cal}$ (mol/g)	R^2
231x10^{-6}	0.043	55x10^{-6}	0.960	1939.9	235x10^{-6}	0.999

3.8. Thermodynamic studies

Thermodynamic parameters are calculated by following equations [40]:

$$K_c = \frac{C_{ads}}{C_e} = \frac{C_o - C_e}{C_e} = \frac{C_o}{C_e} - 1 \quad (11)$$

$$\Delta G^o = -RTlnK_c \quad (12)$$

$$lnK_c = \frac{\Delta S^o}{R} - \frac{\Delta H^o}{RT} \quad (13)$$

Where, C_o the original copper concentration (mol/L), K_c equilibrium constant, C_e remaining concentration in solution at equilibrium (mol/L) and C_{ads} concentration of adsorbed copper

(mol/L). ΔG^o The change in the Gibbes free energy, ΔS^o the entropy and ΔH^o enthalpy. T(K) solution absolute temperature and R gas constant (8.314 $J.mol^{-1}.K^{-1}$). The ΔG^o has a negative value , meaning that the adsorption of copper onto GO/CS was spontaneous, and the slope and intercept of the van't Hoff plot (Figure13) are used to calculate ΔH^o and ΔS^o. Table 4 summarizes the thermodynamic results, which show that a positive entropy value indicates an increase in randomness and a positive enthalpy value indicates that the adsorption reaction was endothermic.

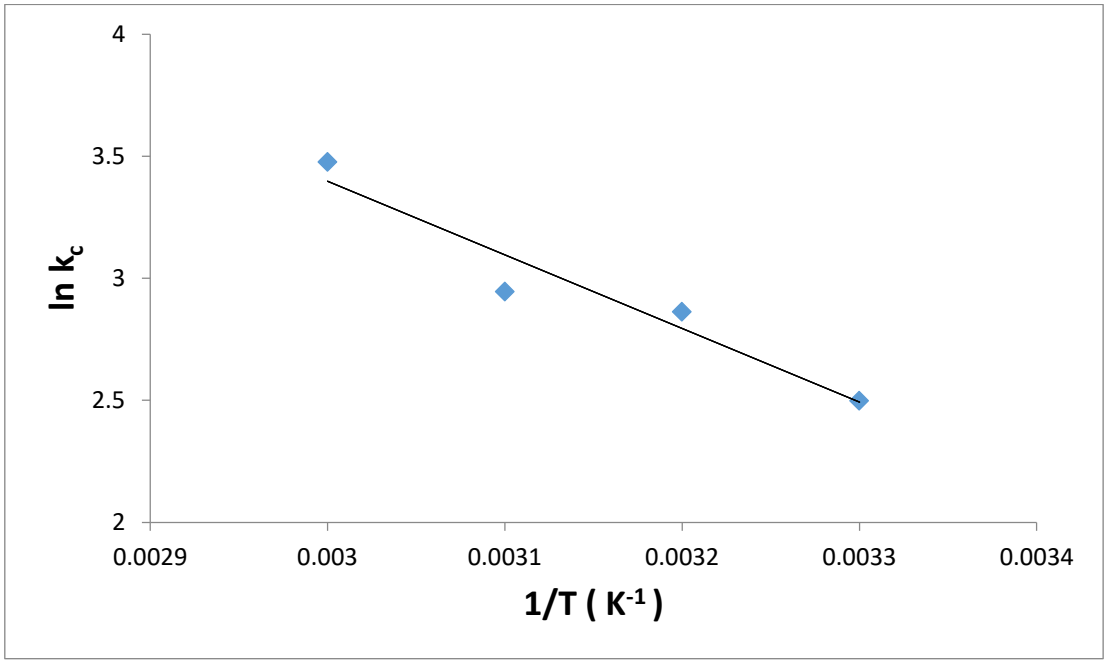

Figure 13- Van't Hoff plot of Cu(II) onto GO/CS.

Table 4- Values of thermodynamic parameters for the adsorption of Cu(II) onto GO/CS.

T(K)	ΔG^o (kJ/mol)	ΔH^o (kJ/mol)	ΔS^o (J/mol.K)
298	-6.187	+25.075	+0.103
308	-7.330		
318	-7.784		
328	-9.476		

4. Conclusions

A graphene oxide/chitosan nanocomposite was synthesized and used to remove copper from industrial wastewater. To describe adsorption isotherms, the Langmuir and Freundlich models were used, with the Freundlich model providing the best fit for equilibrium data. Thermodynamic experiments indicate that the adsorption process endothermic and spontaneous.

References

[1] K. Y. Hor *et al.*, "Evaluation of physicochemical methods in enhancing the adsorption performance of natural zeolite as low-cost adsorbent of methylene blue dye from wastewater," *J. Clean. Prod.*, vol. 118, pp. 197–209, 2016.

[2] C. Dong, J. Lu, B. Qiu, B. Shen, M. Xing, and J. Zhang, "Developing stretchable and graphene-oxide-based hydrogel for the removal of organic pollutants and metal ions," *Appl. Catal. B Environ.*, vol. 222, no. October 2017, pp. 146–156, 2018, doi: 10.1016/j.apcatb.2017.10.011.

[3] H. Hu, X. Li, P. Huang, Q. Zhang, and W. Yuan, "Efficient removal of copper from wastewater by using mechanically activated calcium carbonate," *J. Environ. Manage.*, vol. 203, pp. 1–7,

2017, doi: 10.1016/j.jenvman.2017.07.066.

[4] Y. Zou *et al.*, "Environmental Remediation and Application of Nanoscale Zero-Valent Iron and Its Composites for the Removal of Heavy Metal Ions: A Review," *Environ. Sci. Technol.*, vol. 50, no. 14, pp. 7290–7304, 2016, doi: 10.1021/acs.est.6b01897.

[5] S. S. Al Moharbi, M. G. Devi, B. M. Sangeetha, and S. Jahan, "Studies on the removal of copper ions from industrial effluent by Azadirachta indica powder," *Appl. Water Sci.*, vol. 10, no. 1, pp. 1–10, 2020, doi: 10.1007/s13201-019-1100-z.

[6] A. Pal, J. Jayamani, and R. Prasad, "An urgent need to reassess the safe levels of copper in the drinking water: Lessons from studies on healthy animals harboring no genetic deficits," *Neurotoxicology*, vol. 44, pp. 58–60, 2014, doi: 10.1016/j.neuro.2014.05.005.

[7] F. Fu and Q. Wang, "Removal of heavy metal ions from wastewaters: A review," *J. Environ. Manage.*, vol. 92, no. 3, pp. 407–418, 2011, doi: 10.1016/j.jenvman.2010.11.011.

[8] E. Bazrafshan, L. Mohammadi, A. Ansari-Moghaddam, and A. H. Mahvi, "Heavy metals removal from aqueous environments by electrocoagulation process - A systematic review," *J. Environ. Heal. Sci. Eng.*, vol. 13, no. 1, 2015, doi: 10.1186/s40201-015-0233-8.

[9] C. F. Carolin, P. S. Kumar, A. Saravanan, G. J. Joshiba, and M. Naushad, "Efficient techniques for the removal of toxic heavy metals from aquatic environment: A review," *J. Environ. Chem. Eng.*, vol. 5, no. 3, pp. 2782–2799, 2017, doi: 10.1016/j.jece.2017.05.029.

[10] A. Li *et al.*, "An environment-friendly and multi-functional absorbent from chitosan for organic pollutants and heavy metal ion," *Carbohydr. Polym.*, vol. 148, pp. 272–280, 2016, doi: 10.1016/j.carbpol.2016.04.070.

[11] I. Younes and M. Rinaudo, "Chitin and chitosan preparation from marine sources. Structure, properties and applications," *Mar. Drugs*, vol. 13, no. 3, pp. 1133–1174, 2015, doi: 10.3390/md13031133.

[12] [A. Sumaila, M. M. Ndamitso, Y. A. Iyaka, A. S. Abdulkareem, J. O. Tijani, and M. O. Idris, "Extraction and Characterization of Chitosan from Crab Shells: Kinetic and Thermodynamic Studies of Arsenic and Copper Adsorption from Electroplating Wastewater," *Iraqi J. Sci.*, pp. 2156–2171, 2020.

[13] G. Rojas, J. Silva, J. A. Flores, A. Rodriguez, M. Ly, and H. Maldonado, "Adsorption of chromium onto cross-linked chitosan," *Sep. Purif. Technol.*, vol. 44, no. 1, pp. 31–36, 2005, doi: 10.1016/j.seppur.2004.11.013.

[14] V. Nejadshafiee and M. R. Islami, "Intelligent-activated carbon prepared from pistachio shells precursor for effective adsorption of heavy metals from industrial waste of copper mine," *Environ. Sci. Pollut. Res.*, vol. 27, no. 2, pp. 1625–1639, 2020, doi: 10.1007/s11356-019-06732-4.

[15] J. Xu *et al.*, "A review of functionalized carbon nanotubes and graphene for heavy metal adsorption from water: Preparation, application, and mechanism," *Chemosphere*, vol. 195, pp. 351–364, 2018, doi: 10.1016/j.chemosphere.2017.12.061.

[16] A. Bashir *et al.*, "Removal of heavy metal ions from aqueous system by ion-exchange and biosorption methods," *Environ. Chem. Lett.*, vol. 17, no. 2, pp. 729–754, 2019, doi: 10.1007/s10311-018-00828-y.

[17] J. Hao, L. Ji, C. Li, C. Hu, and K. Wu, "Rapid, efficient and economic removal of organic dyes and heavy metals from wastewater by zinc-induced in-situ reduction and precipitation of graphene oxide," *J. Taiwan Inst. Chem. Eng.*, vol. 88, pp. 137–145, 2018, doi: 10.1016/j.jtice.2018.03.045.

[18] M. S. Samuel, J. Bhattacharya, S. Raj, N. Santhanam, H. Singh, and N. D. P. Singh, "Efficient removal of Chromium(VI) from aqueous solution using chitosan grafted graphene oxide (CS-GO) nanocomposite," *Int. J. Biol. Macromol.*, no. Vi, p. #pagerange#, 2018, doi: 10.1016/j.ijbiomac.2018.09.170.

[19] W. S. Hummers and R. E. Offeman, "Preparation of Graphitic Oxide," *J. Am. Chem. Soc.*, vol. 80, no. 6, p. 1339, Mar. 1958, doi: 10.1021/ja01539a017.

[20] K. Zhang, R. Hu, G. Fan, and G. Li, "Graphene oxide/chitosan nanocomposite coated quartz crystal microbalance sensor for detection of amine vapors," *Sensors Actuators, B Chem.*, vol. 243, pp. 721–730, 2017, doi: 10.1016/j.snb.2016.12.063.

[21] R. Ahmad and R. Kumar, "Adsorption studies of hazardous malachite green onto treated ginger waste," *J. Environ. Manage.*, vol. 91, no. 4, pp. 1032–1038, 2010, doi: 10.1016/j.jenvman.2009.12.016.

[22] M. S. Muda *et al.*, "Chitosan-graphene oxide nanocomposites as water-solubilising agents for rotenone pesticide," *J. Mol. Liq.*, vol. 318, p. 114066, 2020, doi: 10.1016/j.molliq.2020.114066.

[23] A. Kaushal, S. K. Dhawan, and V. Singh, "Determination of crystallite size, number of graphene layers and defect density of graphene oxide (GO) and reduced graphene oxide (RGO)," *AIP Conf. Proc.*, vol. 2115, no. July, pp. 1–5, 2019, doi: 10.1063/1.5112945.

[24] F. T. L. Muniz, M. A. R. Miranda, C. Morilla dos Santos, and J. M. Sasaki, "The Scherrer equation and the dynamical theory of X-ray diffraction," *Acta Crystallogr. Sect. A Found. Adv.*, vol. 72, no. 3, pp. 385–390, 2016.

[25] S. C. Lau *et al.*, "Enhanced biocatalytic esterification with lipase-immobilized chitosan/graphene oxide beads," *PLoS One*, vol. 9, no. 8, 2014, doi: 10.1371/journal.pone.0104695.

[26] J. Shah and M. R. Jan, "Magnetic chitosan graphene oxide composite for solid phase extraction of phenylurea herbicides," *Carbohydr. Polym.*, vol. 199, pp. 461–472, 2018.

[27] A. Farhan, R. Jassim, and N. Kadhim, "The Removal of Zinc from Aqueous Solutions Using Malvaparviflora," *Baghdad Sci. J.*, vol. 13, no. 3, pp. 482–488, 2016, doi: 10.21123/bsj.2016.13.3.0482.

[28] K. A. Kareem, "Removal and Recovery of Methylene Blue Dye from Aqueous Solution using Avena Fatua Seed Husk," *ibn Al-Haitham J. Pure Appl. Sci.*, vol. 29, no. 3, pp. 179–194, 2016.

[29] S. Sonawane, P. Chaudhari, S. Ghodke, S. Phadtare, and S. Meshram, "Ultrasound assisted adsorption of basic dye onto organically modified bentonitenanoclay," *J. Sci. Ind. Res. (India).*, vol. 68, no. 2, pp. 162–167, 2009.

[30] M. Rafatullah, O. Sulaiman, R. Hashim, and A. Ahmad, "Adsorption of copper (II), chromium (III), nickel (II) and lead (II) ions from aqueous solutions by meranti sawdust," *J. Hazard. Mater.*, vol. 170, no. 2–3, pp. 969–977, 2009, doi: 10.1016/j.jhazmat.2009.05.066.

[31] M. T. Yagub, T. K. Sen, S. Afroze, and H. M. Ang, "Dye and its removal from aqueous solution by adsorption: A review," *Adv. Colloid Interface Sci.*, vol. 209, pp. 172–184, 2014, doi: 10.1016/j.cis.2014.04.002.

[32] M. A. Al-Ghouti and D. A. Da'ana, "Guidelines for the use and interpretation of adsorption isotherm models: A review," *J. Hazard. Mater.*, vol. 393, no. November 2019, p. 122383, 2020, doi: 10.1016/j.jhazmat.2020.122383.

[33] I. Belbachir and B. Makhoukhi, "Adsorption of Bezathren dyes onto sodic bentonite from aqueous solutions," *J. Taiwan Inst. Chem. Eng.*, vol. 75, pp. 105–111, 2017, doi: 10.1016/j.jtice.2016.09.042.

[34] L. Liu, X. B. Luo, L. Ding, and S. L. Luo, *Application of Nanotechnology in the Removal of Heavy Metal From Water*. Elsevier Inc., 2018.

[35] D. A.O, "Langmuir, Freundlich, Temkin and Dubinin–Radushkevich Isotherms Studies of Equilibrium Sorption of Zn 2+ Unto Phosphoric Acid Modified Rice Husk," *IOSR J. Appl. Chem.*, vol. 3, no. 1, pp. 38–45, 2012, doi: 10.9790/5736-0313845.

[36] A. B. D. Nandiyanto *et al.*, "Adsorption Isotherm of Carbon Microparticles Prepared from Pumpkin (Cucurbita maxima) Seeds for Dye Removal," *Iraqi J. Sci.*, pp. 1404–1414, 2021.

[37] J. Y. Lim, N. M. Mubarak, E. C. Abdullah, S. Nizamuddin, M. Khalid, and Inamuddin, "Recent trends in the synthesis of graphene and graphene oxide based nanomaterials for removal of heavy metals — A review," *J. Ind. Eng. Chem.*, vol. 66, pp. 29–44, 2018, doi: 10.1016/j.jiec.2018.05.028.

[38] E. . M. Al-kinani, "Studies on Removal of Hexavalent Chromium Ion from Aqueous Solution Using Polyaniline Composite," *J. Al-Nahrain Univ.*, vol. 19, no. 2, pp. 58–68, 2016, doi: 10.22401/jnus.19.2.08.

[39] Y.-S. Ho and G. McKay, "Pseudo-second order model for sorption processes," *Process Biochem.*, vol. 34, no. 5, pp. 451–465, 1999.

[40] K. A. Al-Rudaini, "Adsorption Removal of Rhodamine-B Dye from Aqueous Solution Using Rhamnus Stone as Low Cost Adsorbent," *J. Al-Nahrain Univ.*, vol. 20, no. 1, pp. 32–41, 2017, doi: 10.22401/jnus.20.1.05.